Dr. D.V. Konarev, Institute of Problems of Chemical Physics RAS,

Chernogolovka, Moscow region 142432, Russia.

FAX : +007-096- 515-54-20; E-mail: konarev3@yandex.ru

Magnetic and optical properties of layered $(Me_4P^+)[M^{IV}O(Pc^{\bullet 3-})]^{\bullet -}(TPC)_{0.5} \cdot C_6H_4Cl_2$ salts (M = Ti and V) composed of π-stacking dimers of titanyl and vanadyl phthalocyanine radical anions

Dmitri Valentinovich Konarev,*† Yoshiaki Nakano, §,# Salavat Salimyanovich Khasanov,‡ Alexey

V. Kuzmin, ‡ Manabu Ishikawa, §,# Akihiro Otsuka, §,# Hideki Yamochi, §,# Gunzi Saito‖, ¶ Rimma

Nikolaevna Lyubovskaya†

†Institute of Problems of Chemical Physics RAS, Chernogolovka, Moscow region, 142432 Russia;

email: konarev3@yandex.ru, FAX: +7 49652-21852; ‡Institute of Solid State Physics RAS,

Chernogolovka, Moscow region, 142432 Russia; §Department of Chemistry, Graduate School of

Science, Kyoto University, Sakyo-ku, Kyoto 606-8502, Japan; #Research Center for Low

Temperature and Materials Sciences, Kyoto University, Sakyo-ku, Kyoto 606-8501, Japan;‖Faculty

of Agriculture, Meijo University, 1-501 Shiogamaguchi, Tempaku-ku, Nagoya 468-8502, Japan;

¶Toyota Physical and Chemical Research Institute, 41-1, Yokomichi, Nagakute, Aichi 480-1192,

Japan

ABSTRACT: Two isostructural salts with radical anions of titanyl and vanadyl phthalocyanines $(Me_4P^+)[M^{IV}O(Pc^{\bullet 3-})]^{\bullet -}(TPC)_{0.5} \cdot C_6H_4Cl_2$ (M = Ti (**1**), V (**2**)), where TPC is triptycene, were obtained. These salts contain phthalocyanine layers composed of the $[(M^{IV}OPc^{\bullet 3-})]^{\bullet -}_2$ dimers with strong π-π intradimer interaction. The reduction of metal phthalocyanines was centered on the Pc macrocycles providing the appearance of new bands in the NIR range and a blue shift of Q- and Soret bands. That results in the alternation of shorter and longer $C-N_{imine}$ bonds in $Pc^{\bullet 3-}$. Only one $S=1/2$ spin is delocalized over $Pc^{\bullet 3-}$ in **1** providing $\chi_M T$ value of 0.364 emuKmol^{-1} at 300K. Salt **1** showed antiferromagnetic behavior approximated by the Heisenberg model for isolated pairs of antiferromagnetically interacting spins with exchange interaction of J/k_B = -123.0K. The $\chi_M T$ value for **2** is equal to 0.617 emuKmol^{-1} at 300K to show the contribution of two $S=1/2$ spins localized on V^{IV} and delocalized over $Pc^{\bullet 3-}$. Magnetic behavior of **2** is described by the Heisenberg model for a four-spin system with strong intermolecular coupling between $Pc^{\bullet 3-}$ in $[(V^{IV}OPc^{\bullet 3-})]^{\bullet -}_2$ (J_{inter}/k_B = -105.0K) and weaker intramolecular coupling between the V^{IV} and $Pc^{\bullet 3-}$ (J_{intra}/k_B = -15.2K).

Magnetic and optical properties of layered (Me$_4$P$^+$)[M^{IV}O(Pc$^{•3-}$)]$^{•-}$(TPC)$_{0.5}$·C$_6$H$_4$Cl$_2$ salts (M = Ti and V) composed of π-stacking dimers of titanyl and vanadyl phthalocyanine radical anions

Dmitri Valentinovich Konarev,*[†] Yoshiaki Nakano, [§,#] Salavat Salimyanovich Khasanov,[‡] Alexey V. Kuzmin, [‡] Manabu Ishikawa, [§,#] Akihiro Otsuka, [§,#] Hideki Yamochi, [§,#] Gunzi Saito[||, ¶] Rimma Nikolaevna Lyubovskaya[†]

Institute of Problems of Chemical Physics RAS, Chernogolovka, Moscow region, 142432

 Russia;

Institute of Solid State Physics RAS, Chernogolovka, Moscow region, 142432 Russia;

Department of Chemistry, Graduate School of Science, Kyoto University, Sakyo-ku, Kyoto 606-8502, Japan;

Research Center for Low Temperature and Materials Sciences, Kyoto University, Sakyo-ku, Kyoto 606-8501, Japan;

Faculty of Agriculture, Meijo University, 1-501 Shiogamaguchi, Tempaku-ku, Nagoya 468-8502, Japan;

Toyota Physical and Chemical Research Institute, 41-1, Yokomichi, Nagakute, Aichi 480-1192, Japan

*Corresponding author: Dr. D.V. Konarev, Institute of Problems of Chemical Physics RAS, Chernogolovka, Moscow region 142432, Russia. FAX: +007-496-522-18-52; E-mail: konarev3@yandex.ru.

†Institute of Problems of Chemical Physics RAS.

‡Institute of Solid State Physics RAS.

§Department of Chemistry, Graduate School of Science, Kyoto University.

#Research Center for Low Temperature and Materials Sciences, Kyoto University.

∥Faculty of Agriculture, Meijo University.

¶Toyota Physical and Chemical Research Institute.

ABSTRACT: Two isostructural salts with radical anions of titanyl and vanadyl phthalocyanines $(Me_4P^+)[M^{IV}O(Pc^{\bullet 3-})]^{\bullet -}(TPC)_{0.5} \cdot C_6H_4Cl_2$ (M = Ti (**1**), V (**2**)), where TPC is triptycene, were obtained. These salts contain phthalocyanine layers composed of the $[(M^{IV}OPc^{\bullet 3-})]^{\bullet -}_2$ dimers with strong π-π intradimer interaction. The reduction of metal phthalocyanines was centered on the Pc macrocycles providing the appearance of new bands in the NIR range and a blue shift of Q- and Soret bands. That results in the alternation of shorter and longer $C-N_{imine}$ bonds in $Pc^{\bullet 3-}$. Only one $S=1/2$ spin is delocalized over $Pc^{\bullet 3-}$ in **1** providing $\chi_M T$ value of 0.364 emuKmol^{-1} at 300K. Salt **1** showed antiferromagnetic behavior approximated by the Heisenberg model for isolated pairs of antiferromagnetically interacting spins with exchange interaction of $J/k_B = -123.0$K. The $\chi_M T$ value for **2** is equal to 0.617 emuKmol^{-1} at 300K to show the contribution of two $S=1/2$ spins localized on

V^{IV} and delocalized over $Pc^{\bullet 3-}$. Magnetic behavior of **2** is described by the Heisenberg model for a four-spin system with strong intermolecular coupling between $Pc^{\bullet 3-}$ in $[(V^{IV}OPc^{\bullet 3-})]^{\bullet}_2$ ($J_{inter}/k_B = -105.0K$) and weaker intramolecular coupling between the V^{IV} and $Pc^{\bullet 3-}$ ($J_{intra}/k_B = -15.2K$).

KEYWORDS: titanyl and vanadyl phthalocyanines, reduction, crystal structure, optical and magnetic properties, antiferromagnetic ordering of spins.

INTRODUCTION

Metal phthalocyanine compounds can possess promising optical, conducting and magnetic properties.[1-9] Some phthalocyanine derivatives can be used as sensors and materials for optical, electronic and photoelectronic devices.[1,2] Conducting compounds were obtained by oxidation of metal-free and metal-containing phthalocyanines by iodine or the electrochemical oxidation of axially substituted phthalocyanines anions $[M^{III}PcL_2]^-$ anions (M = Co, Fe; L = CN, Cl, Br).[3-7] Partially oxidized phthalocyanine macrocycles together with a columnar or layered arrangement of π-π stacking provide semiconducting or quasi-one-dimensional metallic conductivity (in some cases down to 4 K).[3-7] The salts with the partially oxidized $[Fe^{III}Pc(CN^-)_2]^-$ anions show giant magnetoresistance.[5-7] Since metal phthalocyanines can contain paramagnetic metals they also used as an active components in the design of magnetic compounds. For example, oxidation of manganese(II) phthalocyanine and substituted naphthalocyanine by tetracyanoethylene yields polymeric compounds with the alternation of the $(Mn^{III}Pc)^+$ and $TCNE^{\bullet-}$ ions. These compounds show ferrimagnetic ordering of spins.[8,9]

Metal phthalocyanines in the reduced states can also exhibit promising magnetic and conducting properties. Theoretical calculations show that non-transition metal phthalocyanines can be metallic or even superconducting at electron doping.[10] Radical anions and dianions of metal phthalocyanines can be obtained at the potentials of -0.4 – -0.8 and -1.0 – -1.4 V, respectively.[11] However, the

number of reduced metal phthalocyanines obtained as crystals is less than twenty.[12-28] That can be due to their high air-sensitivity. Salts with cobalt(I) and iron(I) phthalocyanine and iron(I) hexadecachlorophthalocyanine anions were obtained.[12-17] A series of salts with the $[MPc]^{\bullet-}$ radical anions (M = H_2, Cu^{II}, Ni^{II}, Sn^{II}, Pb^{II}, $In^{III}Br$, $Ti^{IV}O$, $V^{IV}O$),[18-20] $Sn^{IV}Cl_2$,[21] and Mg^{II},[22] and the $[Nb^{IV}O(Pc^{4-})]^{2-}$ dianions[23] are known. There are neutral metal phthalocyanine compounds which formally contain phthalocyanine radical trianions and tetraanions: $Al^{III}(Pc^{\bullet 3-})$,[24,25] $Ga^{III}(Pc^{\bullet 3-})$,[25] $Ge^{IV}(Pc^{4-})$,[26] $Zr^{IV}(Pc^{4-})$[27] and $Sn^{IV}Ph(Pc^{\bullet 3-})$.[28] Negative charge in these compounds is compensated by positive charge of a central metal atom. Compounds with effective magnetic coupling are known for reduced metal phthalocyanines. For example, ferrimagnetic ordering of spins was found in $(Cp*_2Cr^+)[Fe^I(Pc^{2-})]^-\cdot 4C_6H_4Cl_2$ below 4.5 K[13], whereas antiferromagnetic ordering of spins at rather high temperatures was found in the radical anion salts containing $[(MPc^{\bullet 3-})^{\bullet-}]_2$ π-stacking dimers (M = $Ti^{IV}O$, Sn^{II})[20, 29].

In this work, two isostructural layered $(Me_4P^+)[M^{IV}O(Pc^{\bullet 3-})]^{\bullet-}(TPC)_{0.5}\cdot C_6H_4Cl_2$ (M = Ti (**1**), V (**2**)) salts, where TPC is triptycene, have been obtained by a multi-component approach and their crystals structures, optical and magnetic properties have been studied. The $[Ti^{IV}O(Pc^{\bullet 3-})]^{\bullet-}$ and $[V^{IV}O(Pc^{\bullet 3-})]^{\bullet-}$ radical anions are packed in the π-stacking dimers, in which spins interact antiferromagnetically. However, radical anions of titanyl and vanadyl phthalocyanines have different magnetic states which provide different magnetic behavior of the salts. It is important to understand such differences in the design of magnetic assemblies based on radical anions of metal phthalocyanines.

EXPERIMENTAL

Materials. Me_4PBr (Aldrich, 98%), triptycene (Aldrich, 98%), and $[V^{IV}OPc]^0$ (Acros 85%) were used as received.. $Ti^{IV}OPc$ was obtained by 2 hour boiling of $Ti^{IV}Cl_2Pc$ (95%, Aldrich) in wet

pyridine (5% of H_2O) as reported.[30] Sodium fluorenone ketyl was obtained according to Ref.[31] Solvents were purified in argon atmosphere and degassed. o-Dichlorobenzene ($C_6H_4Cl_2$) was distilled over CaH_2 under reduced pressure, benzonitrile was distilled over Na under reduced pressure, and hexane was distilled over Na/benzophenone. All manipulations for the syntheses of **1** and **2** were carried out in an MBraun 150B-G glove box with controlled argon atmosphere and the content of H_2O and O_2 less than 1 ppm. The solvents and crystals were stored in the glove box. Polycrystalline samples of **1** and **2** were placed in 2 mm quartz tubes in anaerobic conditions for EPR and SQUID measurements and sealed under 10^{-5} torr pressure. KBr pellets for IR- and UV-visible-NIR measurements were prepared in the glove box.

Synthesis. Crystals of **1** and **2** were obtained by diffusion technique. A reaction mixture was filtered into a 1.8-cm-diameter, 50 mL glass tube with a ground glass plug, and then 30 mL of hexane was layered over the solution. Slow mixing of the solutions resulted in precipitation of crystals over 1 month. The solvent was then decanted from the crystals, and they were washed with hexane. The compositions of the obtained salts were determined from X-ray diffraction analysis on a single crystal. Several crystals from one synthesis were found to consist of a single crystalline phase. Due to high air sensitivity of **1** and **2**, elemental analysis could not be used to determine the composition because the salts reacted with oxygen in the air before the quantitative oxidation procedure could be performed.

Salts $(Me_4P^+)\{M^{IV}OPc(3-)^{\bullet-}\}(TPC)_{0.5} \cdot C_6H_4Cl_2$ (M = Ti (**1**), V (**2**)) were obtained by the following procedure. The reduction of titanyl(IV) or vanadyl(IV) phthalocyanine ($M^{IV}OPc$, 24.4 mg, 0.042 mmol) in 15 ml of $C_6H_4Cl_2$ with sodium fluorenone ketyl (14 mg, 0.069 mmol) in the presence of the excess of Me_4PBr (25 mg, 0.146 mmol) during 2 hours at 100°C yielded deep blue solution of the salts. Benzonitrile (3 ml) was added, and the mixture was stirred additionally for 2 hours at 100°C. The solution was cooled down to room temperature, and 150 mg of TPC (0.590

mmol) was added to dissolve in the obtained solution at room temperature for 1 hour. The solution was filtered into the tube for diffusion. Crystals of **1** and **2** were obtained as black plates with characteristic copper luster in 65 and 73% yields. Composition of the complexes was determined from X-ray diffraction of single crystals. Several crystals tested from the synthesis showed the same unit cell parameters indicating the formation of one crystal phase.

General. UV-visible-NIR spectra were measured in KBr pellets on a Perkin Elmer Lambda 1050 spectrometer in the 250-2500 nm range. FT-IR spectra were obtained in KBr pellets with a Perkin-Elmer Spectrum 400 spectrometer (400-7800 cm^{-1}). EPR spectra were recorded for polycrystalline samples of **1** and **2** with a JEOL JES-TE 200 X-band ESR spectrometer equipped with a JEOL ES-CT470 cryostat working between room and liquid helium temperatures. A Quantum Design MPMS-XL SQUID magnetometer was used to measure static magnetic susceptibility of **1** and **2** at 100 mT magnetic field in cooling and heating conditions in the 300 − 1.9 K range. A sample holder contribution and core temperature independent diamagnetic susceptibility (χ_d) were subtracted from the experimental values. The χ_d values were estimated by the extrapolation of the data in the high-temperature range by fit the data with the expression: $\chi_M = C/(T - \Theta) + \chi_d$, where C is Curie constant and Θ is Weiss temperature.

Crystal structure determination.

Crystal data of **1** at 100.0(1) K: $C_{104}H_{78}Cl_4N_{16}O_2P_2Ti_2$, $M_r = 1883.36$ g mol^{-1}, black plate, triclinic, $P\overline{1}$, $a = 12.8315(11)$, $b = 13.3759(14)$, $c = 13.9806(18)$ Å, $\alpha = 66.696(11)$, $\beta = 88.101(8)$, $\gamma = 88.872(8)°$, $V = 2202.5(4)$ Å^3, $Z = 1$, $d_{calc} = 1.420$ g·cm^{-3}, $\mu = 0.403$ mm^{-1}, $F(000) = 972$, $2\theta_{max} = 58.592°$, reflections measured 17376, unique reflections 17376, reflections with $I > 2\sigma(I) = 8369$, parameters refined 1217, restraints 621, $R_1 = 0.0972$, $wR_2 = 0.2532$, G.O.F. = 1.007, CCDC 1501234.

Crystal data of **2** at 150(1) K: $C_{104}H_{78}Cl_4N_{16}O_2P_2V_2$, $M_r = 1889.44$ g mol^{-1}, black plate, triclinic,

$P\bar{1}$, $a = 12.8227(6)$, $b = 13.3757(7)$, $c = 13.9746(7)$ Å, $\alpha = 66.450(5)$, $\beta = 88.341(4)$, $\gamma = 88.887(4)^\circ$, $V = 2196.19(19)$ Å^3, $Z = 1$, $d_{calc} = 1.429$ g·cm^{-3}, $\mu = 0.435$ mm^{-1}, $F(000) = 974$, max. $2\theta_{max} = 58.000^\circ$, reflections measured 17724, unique reflections 13570, reflections with $I > 2\sigma(I) = 10870$, parameters refined 1223, restraints 280, $R_1 = 0.0484$, $wR_2 = 0.1085$, G.O.F. = 1.023, CCDC 1501235.

X-ray diffraction data for **1** and **2** were collected on an Oxford diffraction "Gemini-R" CCD diffractometer with graphite monochromated MoK$_\alpha$ radiation using an Oxford Instrument Cryojet system. Raw data reduction to F^2 was carried out using CrysAlisPro, Oxford Diffraction Ltd. The structures of **1** and **2** were solved by direct method and refined by the full-matrix least-squares method against F^2 using SHELX 2013.[32] Non-hydrogen atoms were refined in the anisotropic approximation. Positions of hydrogen were calculated geometrically. Both structures contain two independent C$_6$H$_4$Cl$_2$ molecules. One of two such molecules is disordered in **1** between two orientation with the 0.81(2)/0.19(2) occupancies. Both C$_6$H$_4$Cl$_2$ molecules are disordered in **2** between two orientations with the 0.804(5)/0.196(5) and 0.767(19)/0.233(19) occupancies. To keep the anisotropic thermal parameters of the disordered atoms within reasonable limits the displacement components were restrained using ISOR, SIMU and DELU SHELXL instructions. That resulted in 621 and 280 restraints used for the refinement of the crystal structures of **1** and **2**.

Computational details. DFT and TD-DFT calculations based on the CAM-B3LYP functional[33] were performed using the cc-pVDZ (C, H, N, and O)[34] and cc-pVTZ (Ti and V)[35] basis sets. For the full and partial geometry optimizations on C_{4v}-symmetric [MOPc]^0 and C_{2v}-symmetric [MOPc]$^{\bullet-}$ monomers and [(MOPc)$^{\bullet-}$]$_2$ dimers (M = Ti and V), "Opt = Tight" was specified. In the present DFT calculations, "Int =SuperFineGrid" was specified, and the stabilities of the wave functions were confirmed by specifying the "Stable = Opt" keyword. As for TD-DFT calculations, sixty and forty excited states were calculated for the monomers and dimers, respectively. The subsequent natural bond orbital (NBO) analysis was performed using the NBO program.[36] The computations were

performed with the Gaussian 09 program package.[37]

RESULTS AND DISCUSSION

a. Synthesis. The multi-component approach was developed for preparation of radical anion salts of metal phthalocyanines and fullerenes.[16, 38, 39] In this approach, small organic cations control the charged state of metal phthalocyanine, whereas large organic molecules like triptycene (TPC) control the structure of the salt. TPC molecules form hexagonal vacancies suitable for accommodation of small organic ions providing the formation of layered structures in multi-component complexes of $C_{60}^{\bullet-}$ radical anions and iron(I) phthalocyanine anions.[16, 38, 39] For example, $(Me_4P^+)[Fe^I Pc^{2-}]^- \cdot TPC$ consists of the $(Me_4P^+\text{-}TPC)$ layers and $[(Fe^I Pc^{2-})^-]_2$ π-stacking dimers.[16] By the method for preparation of radical anion salts with titanyl and vanadyl phthalocyanines, the crystals of two isostructural $(Me_4P^+)[M^{IV}O(Pc^{\bullet 3-})]^{\bullet-}(TPC)_{0.5} \cdot C_6H_4Cl_2$ salts (M = Ti (**1**), V (**2**)) were prepared. In the case of **1** and **2,** organic layers have different composition in comparison with the $(Me_4P^+)[Fe^I(Pc^{2-})]^- \cdot TPC$ salt due to that only half of TPC molecules is incorporated into the layers of these salts together with solvent $C_6H_4Cl_2$ molecules.
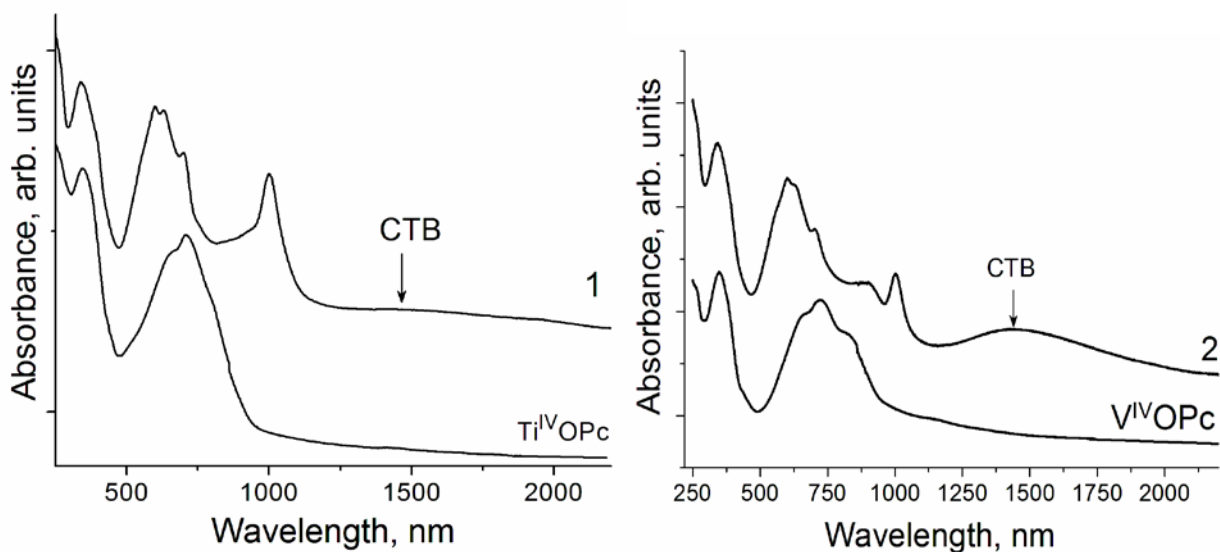
Figure 1. Spectra of starting $Ti^{IV}O(Pc^{2-})$ and $V^{IV}O(Pc^{2-})$, and salts **1** and **2** in the UV-visible-NIR ranges in KBr pellets prepared in anaerobic conditions. Charge transfer bands (CTB) are marked by arrows.

10

b. Optical properties. Spectra of **1** and **2** in the IR- and UV-visible-NIR range are shown in Supporting information (Table S1, Figures S1 and S2) and in Figure 1, respectively. The IR spectra of **1** and **2** are a superposition of the absorption bands of Me_4P^+, $[M^{IV}O(Pc^{•3-})]^{•-}$, TPC and solvent $C_6H_4Cl_2$ molecules (Table S1). Starting $[M^{IV}O(Pc^{2-})]^0$ (M = Ti, V) phthalocyanines have the M=O bonds whose vibrations are manifested at 962 and 963 cm^{-1}, respectively. Upon the formation of $[Ti^{IV}O(Pc^{•3-})]^{•-}$ in **1**, the Ti=O stretching mode was shifted to low frequency and split it into two bands positioned at 923 and 934 cm^{-1}. The low-frequency shift corresponds to the elongation of the Ti=O bond in the radical anion state. However, the formation of $[V^{IV}O(Pc^{•3-})]^{•-}$ in **2** was not accompanied by a shift of this band to show no changes in the V=O bond length in the radical anion state. A similar tendency was found previously for $(Bu_4N^+)[M^{IV}O(Pc^{•3-})]^{•-}$ (M = Ti, V).[20]

The spectra of starting titanyl and vanadyl phthalocyanines are similar. They show intense split Q-bands with maxima at 723 nm (**1**) and 798 nm (**2**) and single Soret bands at 347 (**1**) and 348 nm (**2**). No absorption above 940 nm is observed in the spectra of neutral phthalocyanines (Figure 1). The formation of the salts is accompanied by the appearance of new bands with maxima at 1000 and 1002 nm for **1** and **2,** respectively, characteristic of $Pc^{•3-}$. The Q-bands are noticeably blue shifted in the spectra of the salts as compared with starting phthalocyanines and split into three bands positioned at 700, 627 and 600 (maximum) nm (**1**) and 701, 624, 596 (maximum) nm (**2**). A weak blue shift to 337 and 341 nm is also observed for Soret bands in the spectra of **1** and **2**, respectively. Such shifts are characteristic of metal phthalocyanine radical anion formation by the reduction of the Pc macrocycle.[5] Low-energy broad bands are also manifested in the spectra of **1** and **2** in the NIR range with maxima at 1467 and 1447 nm, respectively (Figure 1, arrows). These bands can be attributed to charge transfer (CT) between $[M^{IV}O(Pc^{•3-})]^{•-}$ in the π-stacking dimers as described in theoretical analysis section.

c. Crystal structures. Crystal structures of **1** and **2** determined at 100 and 150 K, respectively are isostructural and belong to triclinic unit cell. The layered structure consists of the alternation of phthalocyanine layers composed of π-stacking $[(M^{IV}OPc^{\bullet 3-})]^{\bullet-}_2$, π-stacking dimers (Figure 2a) and the Me_4P^+-TPC-$C_6H_4Cl_2$ layers along the *c* axis (Figure 2b). There is a strong shift of non-planar concave shaped phthalocyanines within the dimers. As a result, the distance between metal centers is rather long in the dimers of 7.11 (**1**) and 7.03 Å (**2**). Within a dimer, the planar isoindole units in two $[M^{IV}O(Pc^{\bullet 3-})]^{\bullet-}$ units are located in a face-to-face mode (Figure 3a). Such packing provides effective π-π interaction between them with interplanar distances of only 3.254 and 3.205 Å, and dihedral angles of 0.44 and 0.33º for **1** and **2**, respectively. As a result, multiple short van der Waals C, N···C, N contacts are formed between them of 3.20-3.39 Å (Figures 2b, 3). Strong shift of phthalocyanines in the dimer allows the formation of weak π-stacking between neighboring dimers. To elucidate π-π interaction between phthalocyanines overlap integrals were calculated using crystal structure data for **1** and **2**.[40, 41] Overlap integral (s1) in the π-stacking dimers of 0.0022 for **1** and 0.0017 for **2** (Figure 2b) shows effective π-π interaction between phthalocyanine macrocycles. The interdimer overlap integrals s2 and s3 along the *b* and *a* axes, respectively, are essentially smaller being 0.0001 and 0.0001 for **1** and 0.0001 and 0 for **2**, respectively (Figure 2a). Therefore, the dimers of the $[M^{IV}O(Pc^{\bullet 3-})]^{\bullet-}$ radical anions in **1** and **2** are isolated from each other. For comparison, the overlap integral for previously studied $(Me_4P^+)[Fe^I(Pc^{2-})]^-\cdot$TPC was 0.0047 in the dimers and 0.0001-0.0002 between the dimers.[16]

Geometry of the $Ti^{IV}ON_4$ fragment in **1** is not sensitive to the formation $[Ti^{IV}O(Pc^{\bullet 3-})]^{\bullet -}$ (Table 1), while the geometry of starting $[V^{IV}O(Pc^{2-})]^0$ is unknown to compare it with that in the radical anion state. As also proved by the EPR spectra (vide infra), the reduction of metalphthalocyanines in **1** and **2** is centered on the Pc macrocycles resulting in the shortening and elongation of C-N_{imine} bonds (Table 1) belonging to two oppositely located isoindole units. That can be explained by partial disruption of aromaticity of the macrocycle due to the formation of less stable 19 electron π-system of $Pc^{\bullet 3-}$. Similar changes in the geometry of the Pc macrocycle were observed previously for the $[MPc]^{\bullet -}$ radical anions (M = H_2, Cu^{II}, Ni^{II}, Sn^{II}, Pb^{II}, $Sn^{IV}Cl_2$, $Ti^{IV}O$, $V^{IV}O$) whose reduction is centered on the Pc ligand.[20, 21]
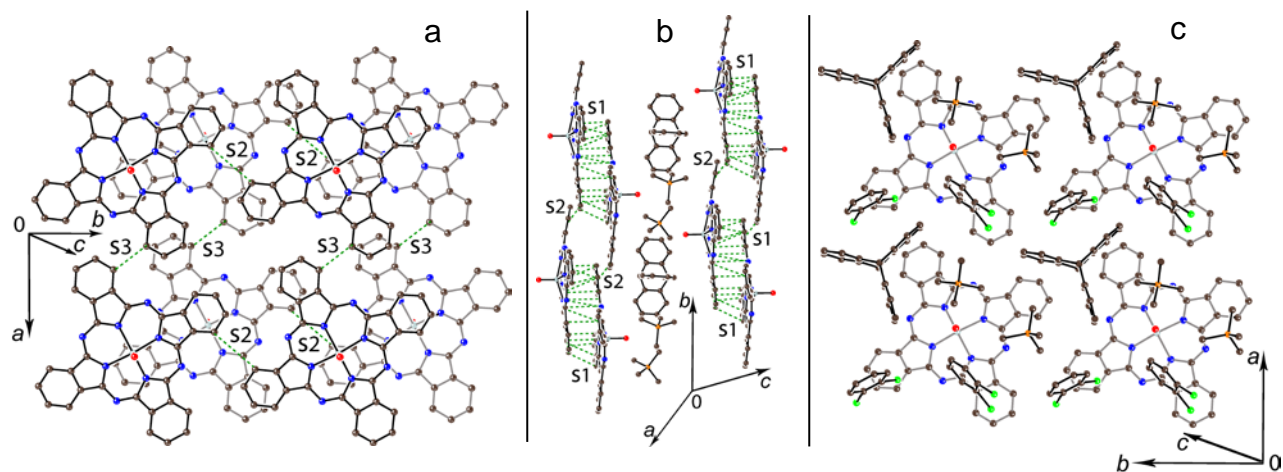
Figure 2. Crystal structure of **1**: (a) view on the phthalocyanine layers consisting of the $[(Ti^{IV}OPc^{\bullet 3-})^{\bullet -}]_2$ π-stacking dimers. The bottom phthalocyanine in a dimer is shown in gray; (b) view along the phthalocyanine layers; (c) projection of organic Me_4P^+-TPC-$C_6H_4Cl_2$ layer on the phthalocyanine layer (only the top phthalocyanine in a dimer is shown). Van der Waals contacts are shown by green dashed lines. Overlap integrals are marked as s1, s2 and s3.

Table 1. Geometric parameters of titanyl and vanadyl phthalocyanines and radical anion salts.

Compound	Average bond length, Å			Displacement of atoms from the 24-atom Pc plane, Å		
	M-$N_{pyrrole}$	C-$N_{pyrrole}$	C-N_{imine} short/long	Metal	Pyrrole nitrogen atoms	Carbon of phenylene groups
$Ti^{IV}O(Pc^{2-})$ Ti=O (1.628(3) Å)[42]	2.067(6)	1.374(6)	1.330(6)	0.778	0.091-0.184	0.165-0.565
$Ti^{IV}O(Pc^{2-})$ Ti=O (1.643(3) Å)[43] both made by Rietveld analysis	2.071(5)	1.375(5)	1.329(5)	0.742	0.076-0.151	0.171-0.411
$(Me_4P^+)[Ti^{IV}O(Pc^{\bullet 3-})]^{\bullet -}(TPC)_{0.5}$ ·$C_6H_4Cl_2$ (**1**)	2.044(13)	1.413(17)	1.291(17)/.1.324(17)	0.734	0.054-0.164	0.023-0.613
Ti=O (1.644(12) and 1.629(12) Å)	2.065(13)	1.382(17)	1.320(17)/1.381(17)	0.729	0.035-0.161	0.075-0.752
$(Bu_4N^+)[Ti^{IV}O(Pc^{\bullet 3-})]^{\bullet -}$ [20] Ti=O (1.640(1) Å)	2.062(1)	1.386(2)	1.325(2)/1.350(2)	0.711	0.084-0.135	0.098-0.574
$(Me_4P^+)[V^{IV}O(Pc^{\bullet 3-})]^{\bullet -}(TPC)_{0.5}$ ·$C_6H_4Cl_2$ (**2**)	2.029(5)	1.383(7)	1.324(7)/1.335(7)	0.666	0.081-0.176	0.152-0.663
V=O (1.603(4) and 1.608(4) Å)	2.027(5)	1.385(7)	1.320(7)/1.334(7)	0.673	0.072-0.164	0.166-0.720
$(Bu_4N^+)[V^{IV}O(Pc^{\bullet 3-})]^{\bullet -}$ [20] V=O (1.598(2) Å)	2.026(2)	1.390(3)	1.312(3)/1.348(3)	0.652	0.068-0.129	0.070-0.576
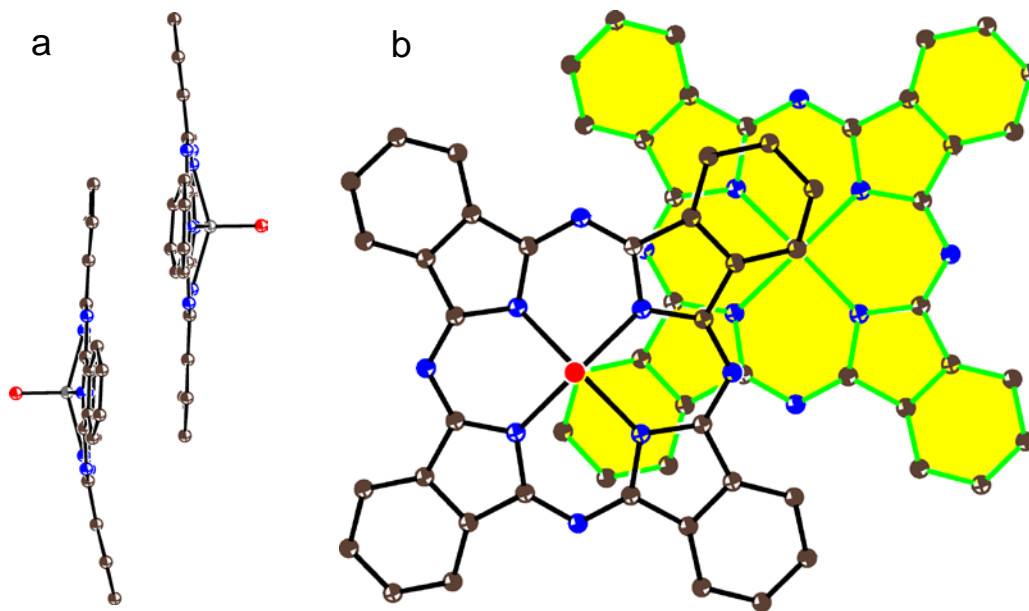
Figure 3. Dimer in **1**: (a) Side view of $[(Ti^{IV}OPc^{\bullet 3-})]^{\bullet -}_2$ π-stacking dimer; (b) overlapping mode for two $[Ti^{IV}O(Pc^{\bullet 3-})]^{\bullet -}$ in dimer. The dimer in **2** shows similar geometry.

Theoretical analysis
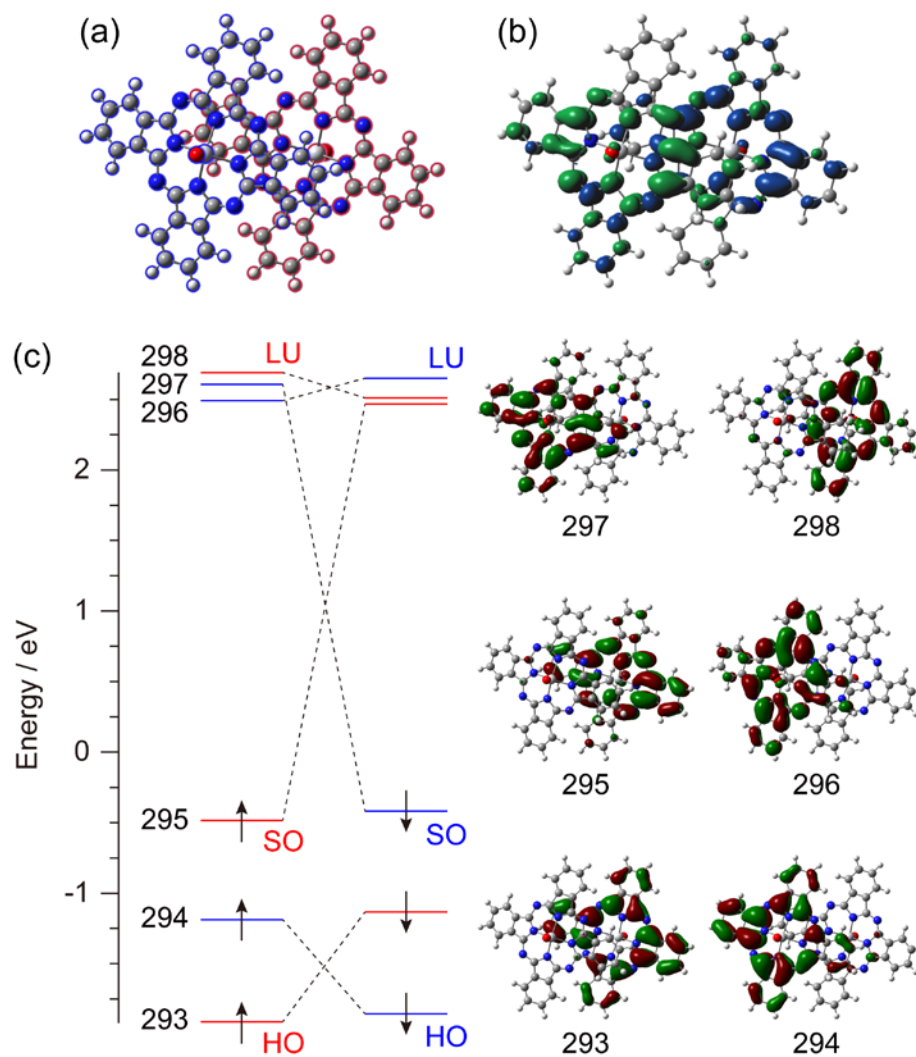
Figure 4. (a) [(TiOPc)$^{\bullet-}$]$_2$ dimer calculated at the UCAM-B3LYP/cc-pVTZ/cc-pVDZ level of theory. [TiOPc]$^{\bullet-}$ monomers are highlighted in red and blue. (b) The isosurface plot for spin density distribution, where the isosurface value is 0.0016 electron/au^3. The isosurfaces in blue and green denote the positive and negative spin density, respectively. (c) Energy diagram for the frontier Kohn-Sham orbitals of the ^1A state. The lines in red and blue are ascribed to the orbital levels mainly contributed by [TiOPc]$^{\bullet-}$ monomers shown in red and blue, respectively. HO, SO, and LU in red and blue indicate the highest occupied, singly occupied, and the lowest unoccupied orbitals of [TiOPc]$^{\bullet-}$ monomers shown in red and blue, respectively. The α-orbitals are shown on the right side.

15

In order to investigate the electronic structure of **1** and **2**, theoretical analyses were performed at the CAM-B3LYP/cc-pVTZ/cc-pVDZ level of theory. Full geometry optimization was done for C_{4v}-symmetric $[MOPc]^0$ and C_{2v}-symmetric $[MOPc]^{\bullet-}$ (M = Ti and V) monomers, whereas the coordinates of hydrogen atoms only were partially optimized for the $[(MOPc)^{\bullet-}]_2$ dimers from the X-ray structures. The total and relative energies, number of imaginary frequency, $\langle S^2 \rangle$ values, and charge and spin density in the monomers and dimers are summarized in Tables S2 and S3.

The energy diagram for the frontier Kohn−Sham orbitals of the $^2B_1$ state in the C_{2v}-symmetric $[TiOPc]^{\bullet-}$ monomer is shown in Figure S7a. The 147th, 148th, and 149th orbitals are the highest occupied (HO), singly occupied (SO), and the lowest unoccupied (LU) orbitals, respectively. The SO and LU orbitals are derived from the doubly degenerate LU orbital, and the HO orbital is derived from the HO orbital of C_{4v}-symmetric $[TiOPc]^0$ (Figure S6). The calculated charges on Ti and O atoms in the $[TiOPc]^{\bullet-}$ are almost the same as those in the $[TiOPc]^0$, while the Pc ligand in the $[TiOPc]^{\bullet-}$ is more negatively charged by one electron than that in the $[TiOPc]^0$ and has a majority of spin density (Table S3). Therefore, the Pc ligand in the $[TiOPc]^{\bullet-}$ can be regarded as an open-shell $Pc^{\bullet 3-}$ radical trianion. The spin density distribution also indicates that the magnetic property stems from the π-radical spin on the Pc moiety (Figure S7b). It is seen from the electrostatic potential map that the isoindole moieties which the SO orbital spreads over are more negatively charged than the other ones (Figure S7c).

The ^1A state in the $[(TiOPc)^{\bullet-}]_2$ dimer was found to be more stable in energy than the ^3A state (Table S2), and the intermolecular antiferromagnetic exchange interaction was estimated to be $J = -196$ K.[33] It is consistent with the observed antiferromagnetic behavior of **1**. The energy diagram for the frontier Kohn−Sham orbitals of the ^1A state in the $[(TiOPc)^{\bullet-}]_2$ dimer is shown in Figure 4. The electronic structure in the $[(TiOPc)^{\bullet-}]_2$ dimer inherits that of the $^2B_1$ state in the $[TiOPc]^{\bullet-}$ monomer. Charge and spin density are also similar to each other for the $[TiOPc]^{\bullet-}$ monomer and the

[(TiOPc)$^{\bullet-}$]$_2$ dimer calculations (Tables S3). The spin density distribution in the [(TiOPc)$^{\bullet-}$]$_2$ dimer spreads over the Pc ligands, and the π-radical spins on the Pc ligands show the intermolecular antiferromagnetic interaction (Figure 4b).
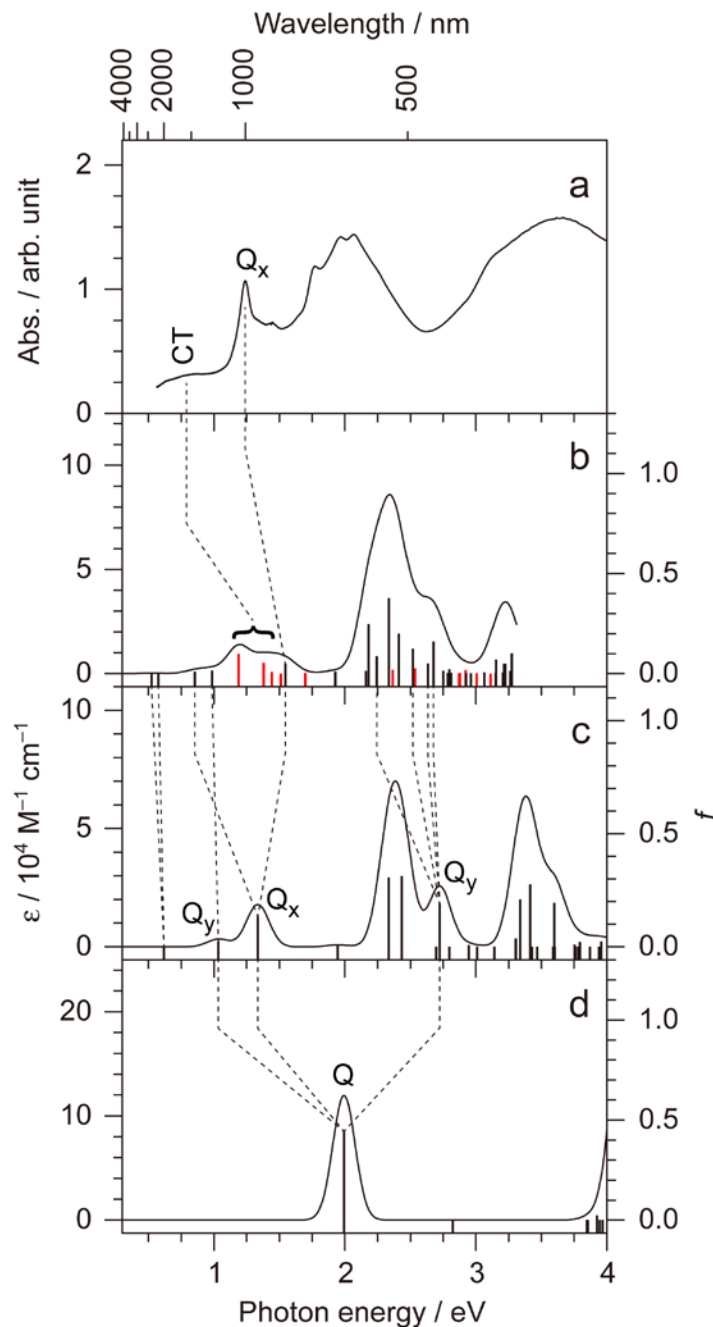
Figure 5. (a) The observed UV-vis-NIR spectrum of **1** in KBr. Calculated spectra of (b) the ^1A state in [(TiOPc)$^{\bullet-}$]$_2$ dimer, (c) the $^2B_1$ state in [TiOPc]$^{\bullet-}$ monomer, and (d) the $^1A_1$ state in [TiOPc]^0 monomer at the TD-CAM-B3LYP/cc-pVTZ/cc-pVDZ level of theory. The SO → SO, SO → LU, and HO → LU charge transfer transitions are indicated as red lines.

17

To obtain further insight into the optical properties of **1**, the excited states of [TiOPc]^0, [TiOPc]$^{\bullet-}$, and [(TiOPc)$^{\bullet-}$]$_2$ were examined based on time-dependent density functional theory (TD-
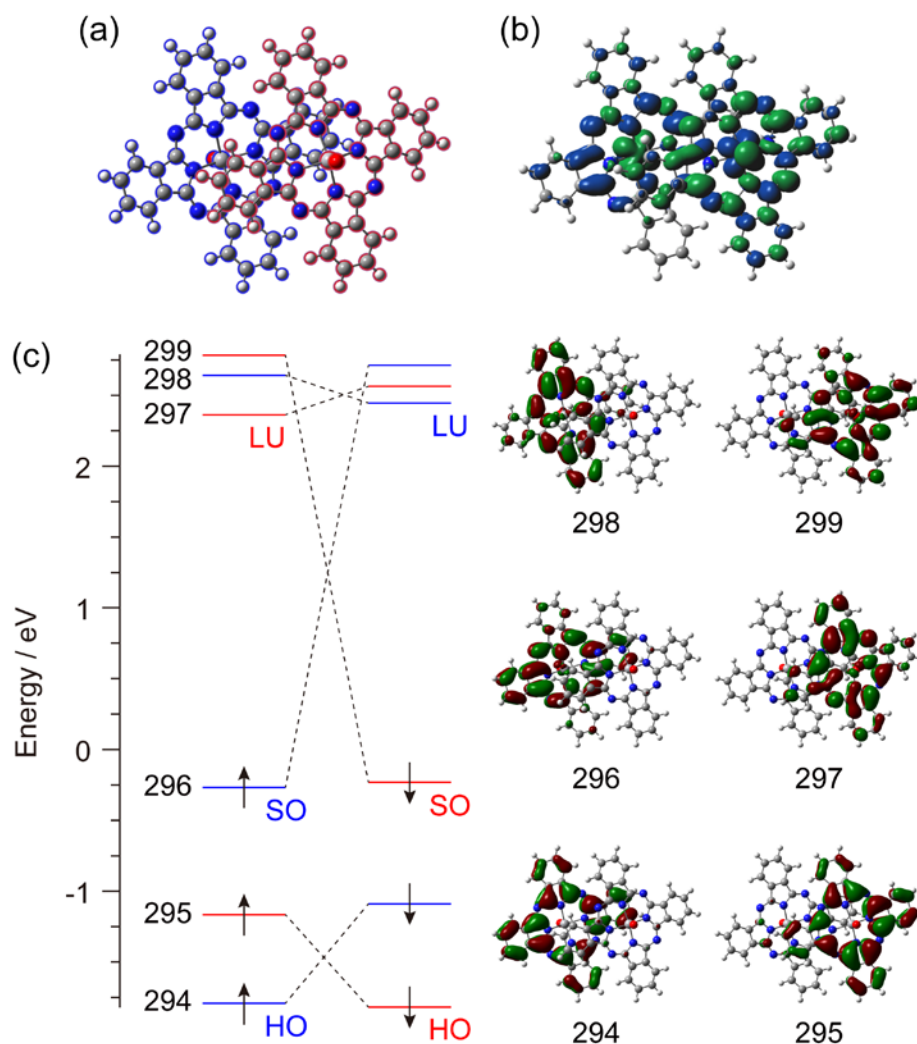
Figure 6. (a) [(VOPc)$^{\bullet-}$]$_2$ dimer calculated at the UCAM-B3LYP/cc-pVTZ/cc-pVDZ level of theory. [VOPc]$^{\bullet-}$ monomers are highlighted in red and blue. (b) The isosurface plot for spin density distribution, where the isosurface value is 0.0016 electron/au^3. The isosurfaces in blue and green denote the positive and negative spin density, respectively. (c) Energy diagram for the frontier Kohn-Sham orbitals of the ground ^1A state. The lines in red and blue are ascribed to the orbital levels mainly contributed by [VOPc]$^{\bullet-}$ monomers in red and blue, respectively. HO, SO, and LU in red and blue indicate the highest occupied, singly occupied, and the lowest unoccupied orbitals of [VOPc]$^{\bullet-}$ monomers in red and blue, respectively. The α-orbitals are shown on the right side.

18

DFT) at the same level of theory. The calculated excitation energies, oscillator strengths, $\langle S^2 \rangle$ values, and assignments on the low-lying excited states of $[TiOPc]^0$, $[TiOPc]^{\bullet-}$, and $[(TiOPc)^{\bullet-}]_2$ are summarized in Tables S4 and S5. The observed UV-vis-NIR spectrum of **1** and the calculated
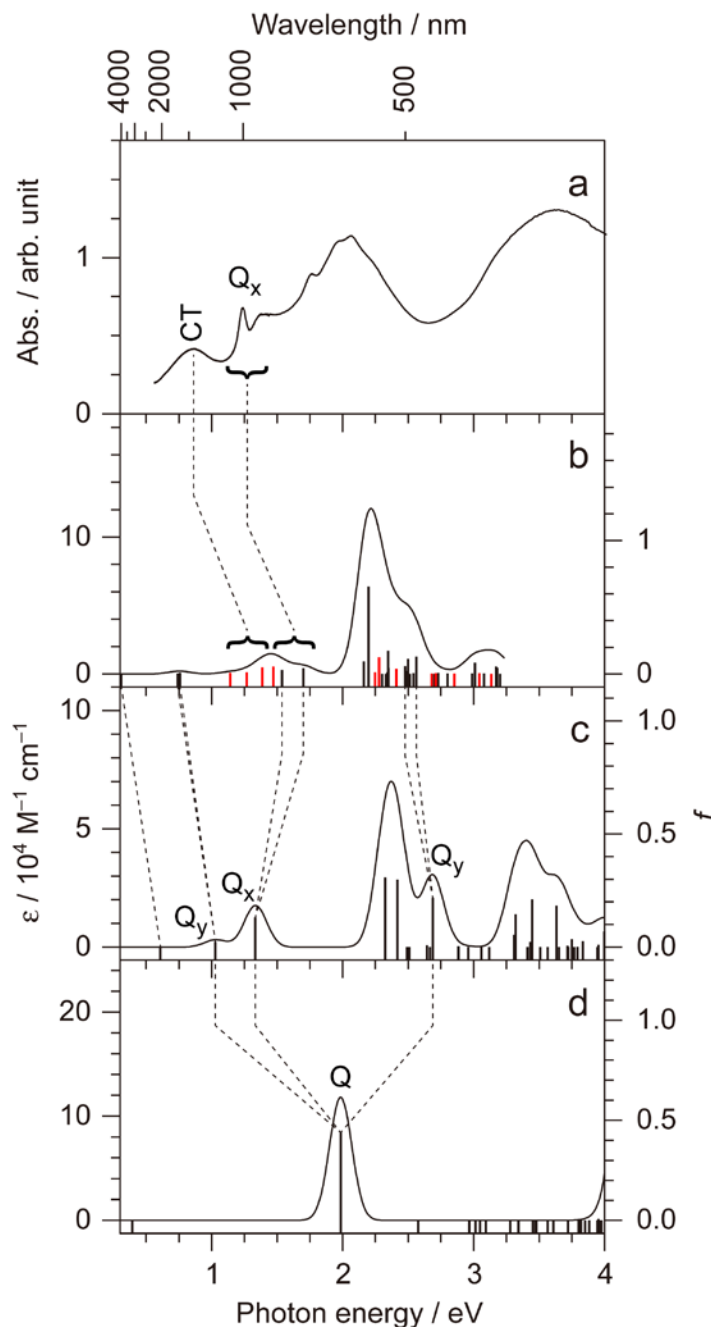
Figure 7. (a) The observed UV-vis-NIR spectrum of **2** in KBr. Calculated spectra of (b) the ^1A state in $[(VOPc)^{\bullet-}]_2$ dimer, (c) the $^1B_2$ state in $[VOPc]^{\bullet-}$ monomer, and (d) the $^2B_1$ state in $[VOPc]^0$ monomer at the TD-CAM-B3LYP/cc-pVTZ/cc-pVDZ level of theory. The SO → SO, SO → LU, and HO → LU charge transfer transitions are indicated as red lines.

19

spectra of $[TiOPc]^0$, $[TiOPc]^{\bullet-}$, and $[(TiOPc)^{\bullet-}]_2$ are compared in Figure 5.

The first excited states of $[TiOPc]^{\bullet-}$ monomer are the SO → LU excitations (Table S4 and Figure 5c). The second/eighth and third excited states are the HO → LU and HO → SO excitations, where these excitations have Q-band character and are denoted as Q_y and Q_x, respectively. These excited states are derived from the splitting of the Q-band in $[TiOPc]^0$ (Figure 5d). The second one with weak oscillator strength, which have little or no impact on the spectral feature, and the eighth one with strong oscillator strength are red- and blue-shifted from the original Q-band, respectively.

As for the $[(TiOPc)^{\bullet-}]_2$ dimer, the spectral feature takes over that of the $[TiOPc]^{\bullet-}$ monomer except for the charge transfer (CT) transitions between $[TiOPc]^{\bullet-}$ monomers (Figure 5). The first and second excited states are the SO → LU excitations (Table S5). The third, fourth, ninth, 14th, 18th, 20th, 21th excited states are related to the Q-band, which are the intramolecular electronic transitions in the $[TiOPc]^{\bullet-}$ monomer. The additional bands that do not exist in the $[TiOPc]^{\bullet-}$ monomer are ascribed to the intermolecular CT transitions. The fifth, seventh, and tenth excited states are the intermolecular SO → SO excitations, the sixth and the eighth ones are intermolecular SO → LU excitations, the 16th and the 19th are intermolecular HO → LU excitations. Comparing the observed UV-vis-NIR spectrum with the calculated ones, the band at 0.84 eV (1467 nm) can be assigned as the CT transition with the character of the intermolecular SO → SO/LU excitation although the CAM-B3LYP functional overestimated the excitation energy. The band at 1.24 eV (1000 nm) can be regarded as intramolecular HO → SO excitations with Q-band character (Q_x).

As for the $[VOPc]^{\bullet-}$ monomer, the $^1B_2$ state was more stable in energy than the $^3B_2$ state (Table S2), and the intramolecular antiferromagnetic exchange interaction was estimated to be $J = -23$ K.[44] The energy diagram for the frontier Kohn−Sham orbitals of the $^1B_2$ state is shown in Fig. S9a. The 146th, 148th, 149th, and 150th orbitals are SO, HO, SO, and LU orbitals, respectively. The 146th orbitals are derived from d orbital of vanadium, and the 149th orbital is derived from the doubly

20

degenerate LU orbital of C_{4v}-symmetric $[VOPc]^0$ (Figure S8). The calculated charges on V and O atoms in $[VOPc]^{\bullet-}$ are almost the same as those in the $[VOPc]^0$, while the Pc ligand in the $[VOPc]^{\bullet-}$ is more negatively charged by one electron than that in the $[VOPc]^0$ and the spin density corresponds to one spin-1/2 (Table S3). Therefore, the Pc ligand in the $[VOPc]^{\bullet-}$ can be regarded as an open-shell $Pc^{\bullet3-}$ radical trianion, and the $[VOPc]^{\bullet-}$ monomer is two spin-1/2 system composed of vanadium d and Pc π-radical spins, which are antiferromagnetically coupled. The spin density distribution also indicates that the magnetic property stems from the π-radical spin on the Pc moiety (Figure S9b). As is the case with the $^2B_1$ state in $[TiOPc]^{\bullet-}$, the electrostatic potential map indicates that the isoindole moieties which accommodate the π-radical spins are more negatively charged than the other ones (Figure S9c).

The ^1A state in the $[(VOPc)^{\bullet-}]_2$ dimer was found to be more stable in energy than the ^3A and ^5A states (Table S2 and Figure S10) that supports the observed antiferromagnetic behavior. The energy diagram for the frontier Kohn−Sham orbitals of the ^1A state in the $[(VOPc)^{\bullet-}]_2$ dimer is shown in Figure 6c. The electronic structure in the $[(VOPc)^{\bullet-}]_2$ dimer inherits that of the $^1B_2$ state in the $[VOPc]^{\bullet-}$ monomer. Charge and spin density are also similar to each other between the $[VOPc]^{\bullet-}$ monomer and the $[(VOPc)^{\bullet-}]_2$ dimer calculations (Tables S3). The spin density distribution in the $[(VOPc)^{\bullet-}]_2$ dimer mainly spreads over the vanadium atoms and the Pc ligands, and the π-radical spins on the Pc ligands show the intermolecular antiferromagnetic interaction (Figure 6b).

As is the case with **1**, the excited states of $[VOPc]^0$, $[VOPc]^{\bullet-}$, and $[(VOPc)^{\bullet-}]_2$ were examined. The calculated excitation energies, oscillator strengths, $\langle S^2 \rangle$ values, and assignments on the low-lying excited states of $[VOPc]^0$, $[VOPc]^{\bullet-}$, and $[(VOPc)^{\bullet-}]_2$ are summarized in Tables S6, S7, and S8. The observed UV-vis-NIR spectrum of **2** and the calculated spectra of $[VOPc]^0$, $[VOPc]^{\bullet-}$, and $[(VOPc)^{\bullet-}]_2$ are compared in Figure 7.

The first excited states of the [VOPc]$^{\bullet-}$ monomer are SO → LU excitations (Table S7 and Figure 7c). The second/tenth and third excited states are HO → LU and HO → SO excitations, which correspond to Q$_y$- and Q$_x$-bands, respectively. As is the case of [(TiOPc)$^{\bullet-}$]$_2$ dimer, the spectral feature of the [(VOPc)$^{\bullet-}$]$_2$ dimer takes over that of the [VOPc]$^{\bullet-}$ monomer except for the CT transitions between the [VOPc]$^{\bullet-}$ monomers (Figure 7). The first and the second excited states are SO → LU excitations (Table S8). The third, fourth, ninth, tenth, 21th, and 26th excited states are related to the Q-band and are the intramolecular electronic transitions in the [VOPc]$^{\bullet-}$ monomer. The additional bands that do not exist in the [VOPc]$^{\bullet-}$ monomer are ascribed to the intermolecular CT transitions. The fifth, sixth excited states are intermolecular SO → LU excitations, the seventh and the eighth are intermolecular SO → SO excitations, the 13th, 14th, and 20th are intermolecular HO → LU excitations. A comparative analysis of the observed UV-vis-NIR spectrum and the
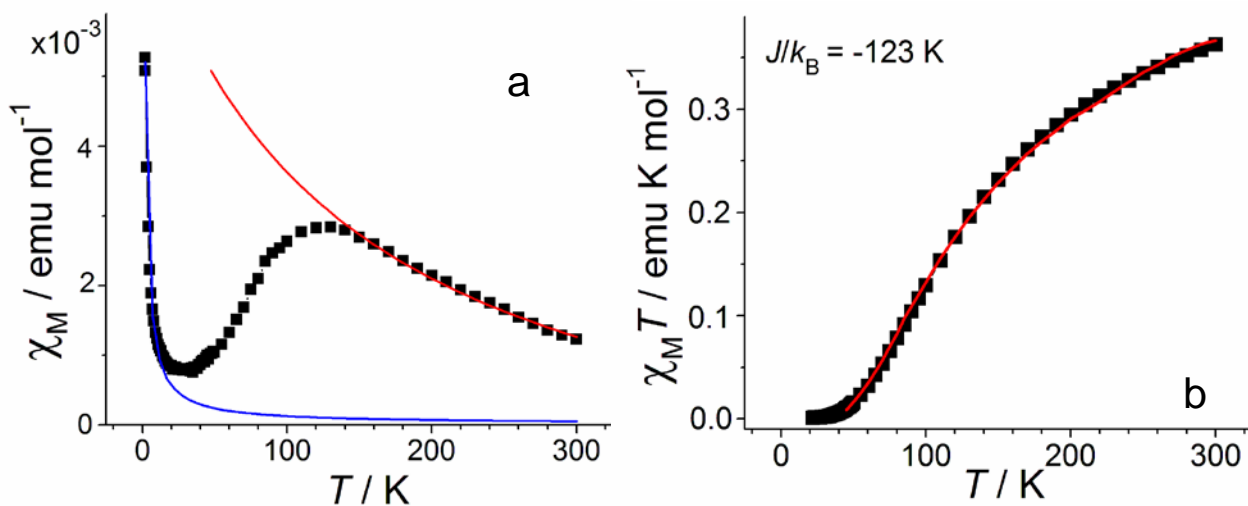
Figure 8. SQUID data for **1**. Temperature dependences of: a). molar magnetic susceptibility and approximation of the data by the Curie-Weiss law in the 160-300 and 1.9-16 K ranges (red and blue curves, respectively); b). temperature dependence of $\chi_M T$ (black squares) and approximation of the data by the Heisenberg model for pairs of antiferromagnetically coupling spins[45] with exchange interaction of J/k_B = -123.0 K (red curve).

calculated ones shows that the band at 0.86 eV (1447 nm) can be assigned as the CT transition with the character of intermolecular SO → SO/LU excitation although the CAM-B3LYP functional overestimated the excitation energy. The band at 1.24 eV (1002 nm) can be regarded as intramolecular HO → SO excitations with the Q-band character (Q_x).

e. Magnetic properties

Magnetic properties of polycrystalline **1** and **2** were studied by SQUID and EPR techniques. Temperature dependence of molar magnetic susceptibility (χ_M) and $\chi_M T$ value in **1** are shown in Figure 8. The $\chi_M T$ value is 0.364 emu K mol^{-1} at 300 K and decreases with temperature (Figure S3a). That indicates the contribution of one $S = 1/2$ spin per formula unit from the Pc$^{•3-}$ macrocycle. The temperature dependence of molar magnetic susceptibility can be described well by two contributions (Figure 8a). One contribution describes magnetic behavior of **1** below 20 K and follows the Curie-Weiss law with nearly zero Weiss temperature and the estimated number of spins of about 1.5% from total amount of [Ti^{IV}O(Pc$^{•3-}$)]$^{•-}$ (Figure 8a, blue curve). Therefore, this contribution originates from small amount of Curie impurities. Subtraction of the contribution of the Curie impurities from
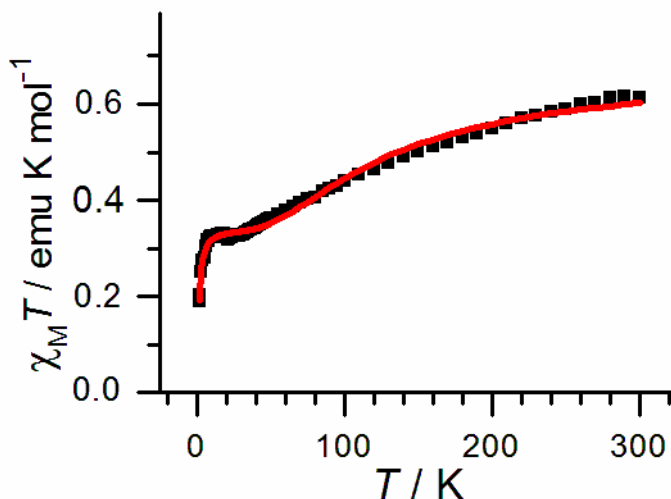
Figure 9. Temperature dependence of $\chi_M T$ (black squares) observed for **2** and approximation of the data by the Heisenberg model for four spin system[46] (red curve).

the experimental data allows one to extract pure contribution from the bulk sample (Figure 8b, red curve). The contribution from the bulk sample can be approximated well by the Heisenberg model for isolated pairs of antiferromagnetically interacting spins[45] with exchange interaction J/k_B = -123.0 K (Figure 8b). This value shows strong antiferromagnetic exchange between the $Pc^{•3-}$ macrocycles in the $[(Ti^{IV}OPc^{•3-})]^{•-}_2$ dimers.

The EPR spectrum of **1** shows an asymmetric signal which can be fit by two Lorentzian lines (Figure S4a). A more intense and broader line has g_1 = 2.0001 and the linewidth (ΔH) of 3.67 mT at 294 K. A narrower line has g_2 = 2.0031 and ΔH = 1.82 mT at 294 K with integral intensity of only 6.8% of total intensities of these two lines. Both lines according to g-factor values[18, 20] can be attributed to $Pc^{•3-}$. However, these lines are essentially broader than those observed for the $(H_2Pc)^{•-}$ radical anions (ΔH = 0.1-0.2 mT)[18, 20]. The signals of both components are shifted to smaller g-values and narrowed with the temperature decrease (Figures S4b and S4c). Total integral intensity of the signal reaches maximum at 140 K, and decreases below this temperature due to antiferromagnetic coupling between spins (Figure S4d). The signal is very weak below 50 K, and can be ascribed to impurities.

The $\chi_M T$ value of **2** is equal to 0.617 emu K mol^{-1} at 300 K (Figure S5a). This value is rather close to the $\chi_M T$ value of 0.750 calculated for the system of two non-interacting S = 1/2 spins (2.45 μ_B). Obviously these spins originate from the V^{IV} centers and the $Pc^{•3-}$ macrocycles having S = 1/2 spin state. The $\chi_M T$ value decreases gradually with lowering temperature below 300 K, and reaches the $\chi_M T$ value of 0.336 emu K mol^{-1} at 7-40 K, indicating the preservation of about one S = 1/2 spin per formula unit at low temperatures (Figure S5a). The $\chi_M T$ value additionally decreases below 7 K, and the minimal $\chi_M T$ value is 0.195 emu K mol^{-1} at 1.9 K. Such magnetic behavior can be well described

by the Heisenberg model for four spin system having stronger and weaker magnetic coupling with exchange interactions $J_1/k_B = -105.0$ K and $J_2/k_B = -15.2$ K (Figure 9). Fitting equation[46] is:

$$\chi = f \frac{Ng^2\mu_B^2}{k_BT} \frac{10\exp(-E_1/k_BT)+2\exp(-E_2/k_BT)+2\exp(-E_3/k_BT)+2\exp(-E_4/k_BT)}{5\exp(-E_1/k_BT)+3\exp(-E_2/k_BT)+3\exp(-E_3/k_BT)+3\exp(-E_4/k_BT)+\exp(-E_5/k_BT)+\exp(-E_6/k_BT)}$$

$E_1 = -J_2 - J_1/2$; $E_2 = J_2 - J_1/2$; $E_3 = J_1/2 + (J_2^2 + J_1^2)^{1/2}$; $E_4 = J_1/2 - (J_2^2 + J_1^2)^{1/2}$; $E_5 = J_2 + J_1/2 + (4J_2^2 - 2J_2J_1 + J_1^2)^{1/2}$; $E_6 = J_2 + J_1/2 - (4J_2^2 - 2J_2J_1 + J_1^2)^{1/2}$ and $f = 0.457$, $g = 2$ (fix), $J_1/k_B = -105.0$ K, $J_2/k_B = -15.2$ K.

Stronger magnetic coupling ($J_1/k_B = -105.0$ K) can be attributed to intermolecular interactions between $Pc^{\bullet 3-}$ in the $[(V^{IV}OPc^{\bullet 3-})]^{\bullet-}_2$ π-stacking dimers (J_{inter}) since this value is close to that in **1** with $J/k_B = -123$ K between $Pc^{\bullet 3-}$ in the $[(Ti^{IV}OPc^{\bullet 3-})]^{\bullet-}_2$ π-stacking dimers. Slightly weaker exchange coupling in **2** in comparison with **1** can be due to smaller overlap integrals between phthalocyanine macrocycles. Therefore, weaker intramolecular coupling between V^{IV} and $Pc^{\bullet 3-}$ spins within the $[(V^{IV}OPc^{\bullet 3-})]^{\bullet-}$ radical anions has the value of $J_{intra}/k_B = -15.2$ K. These data indicate strong magnetic coupling between spins delocalized over the $Pc^{\bullet 3-}$ macrocycles in the dimers and ~7 times weaker intramolecular coupling between the V^{IV} and $Pc^{\bullet 3-}$ spins within one $[V^{IV}OPc^{\bullet 3-}]^{\bullet-}$ radical anion. As a result, the spins of $Pc^{\bullet 3-}$ disappear at low temperatures due to strong antiferromagnetic coupling preserving weakly antiferromagnetically coupled V^{IV} spins down to 1.9 K. Obviously, weak intramolecular coupling is characteristic of metal phthalocyanine radical anions containing one spin localized on the metal center and another spin delocalized over the $Pc^{\bullet 3-}$ macrocycle. Indeed, weak intramolecular coupling is observed in $(TBA^+)[V^{IV}O(Pc^{\bullet 3-})]^{\bullet-}$ within isolated $[V^{IV}O(Pc^{\bullet 3-})]^{\bullet-}$ radical anions since Weiss temperature was only -9.6 K.[20] Similarly, only weak intramolecular coupling was found in isolated $[Cu^{II}(Pc^{\bullet 3-})]^{\bullet-}$ radical anions containing two paramagnetic Cu^{II} and $Pc^{\bullet 3-}$ species. In this case, Weiss temperature was only -4 K.[20]

Salt **2** shows broad signal from room temperature down to 4.4 K. The signal is well described by a combination of two lines in all studied temperature range with the main component at $g_1 = 1.9954$ ($\Delta H = 25.32$ mT) and weaker component at $g_2 = 2.0002$ ($\Delta H = 10.49$ mT) (298 K, Figure 10a). The broadening and the g-factor shift are observed for the components at the temperature decrease: $g_1 = 2.0111$ ($\Delta H = 27.3$ mT) and $g_2 = 1.9832$ ($\Delta H = 31.22$ mT) (6.9 K, Figure 10b). The EPR signals (main component at the least) should come from the contribution of both paramagnetic V^{IV} and $Pc^{\bullet 3-}$ species. The observed g-factor value ($g_1 = 1.9954$) is approximately intermediate between those characteristic of V^{IV} and $Pc^{\bullet 3-}$ is regarded as the result of exchange interaction. In fact, for example, $[V^{IV}OPc^{2-}]^0$ has a very broad signal from V^{IV} with the main component at $g = 1.9858$ at room temperature[20] but the EPR signal from $Pc^{\bullet 3-}$ in the salts with the $[H_2Pc^{\bullet 3-}]^{\bullet -}$ radical anions has $g = 2.0033$ at room temperature.[18] Previously, one signal was also observed in $(TBA^+)[V^{IV}OPc^{\bullet 3-}]^{\bullet -}$ with $g = 1.9918$ ($\Delta H = 7.8$ mT).[20]

Contribution of the $Pc^{\bullet 3-}$ spins disappears at low temperatures due to strong antiferromagnetic coupling, and that allows the observation of hyperfine splitting (HFS) of the EPR signal which is
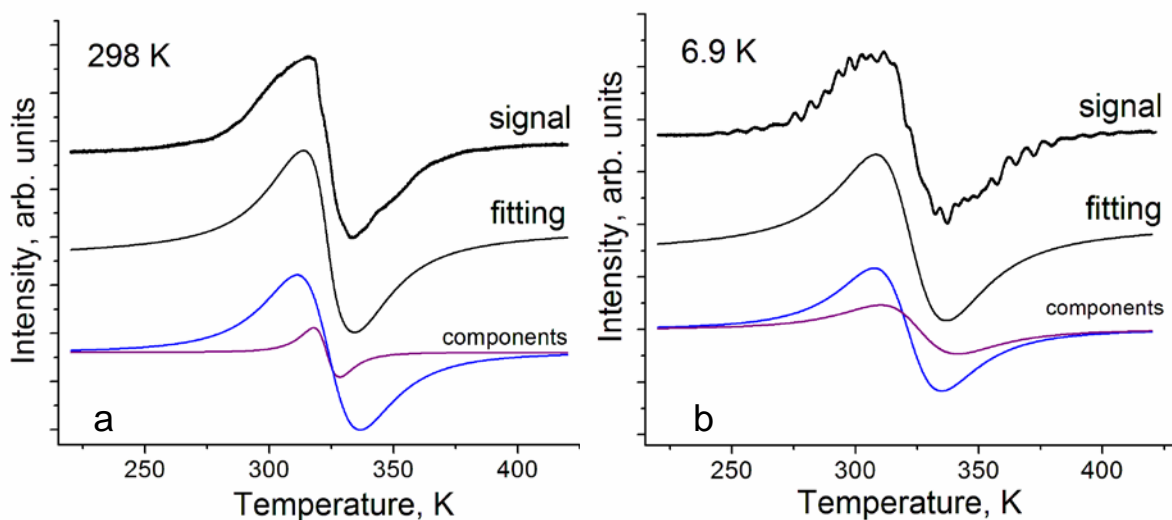
Figure 10. EPR signal of polycrystalline **2** at 298 (a) and 6.9 K (b). Fitting of the signal by two Lorentzian lines is shown below.

partially resolved below 60 K (Figure 10b shows spectrum at 6.9 K). This splitting can originate from the interaction of the V^{IV} spins with the ^{51}V nuclei having $I = 7/2$ nuclear spin. Generally, such spitting generates 8 lines or two sets from 8 lines when signal has two components with $g_{\parallel}$ and $g_{\perp}$.[47-50] The number of lines is increased from 8 to 15 in the $[V^{IV}OPc]_2$ dimers.[51] At least 30 lines are manifested in the spectrum of **2** (Figure 10b). Most probably that is caused by a superposition of the two components of EPR signal in the $[(V^{IV}OPc^{\bullet 3-})]^{\bullet-}_2$ dimers. Separation between the lines is not uniform and varies within 4.6-8.8 mT with the average value of 6.6 mT. Generally, HFS for EPR signal from V^{IV} results in the larger line separation of 9.7-17 mT[47-50] but this separation decreases to 3.2 mT in the dimeric structures[51]. Nitrogen hyperfine splitting constants are reported as only 0.28-0.29 mT in vanadyl porphyrin[49] and 0.25-0.30 mT in vanadyl phthalocyanine[50]. The fact that such a small HFS is not manifested in **2** supports the scenario that the observed HPS stems not from nitrogen but from ^{51}V nuclei ($I = 7/2$) and the dimerization.

CONCLUSION

Thus, two new layered isostructural salts $(Me_4P^+)[M^{IV}OPc^{\bullet 3-}]^{\bullet-}(TPC)_{0.5} \cdot C_6H_4Cl_2$ (M = Ti (**1**), V (**2**)) have been obtained. All data indicate the formation of negatively charged $Pc^{\bullet 3-}$ radical trianions, whereas central metal atoms preserve their charged state to be diamagnetic Ti^{IV} ($S = 0$) and paramagnetic V^{IV} ($S = 1/2$). In these salts, $[M^{IV}OPc^{\bullet 3-}]^{\bullet-}$ radical anions form the $\{[M^{IV}OPc^{\bullet 3-}]^{\bullet-}\}_2$ π-stacking dimers with efficient intradimer π-π interactions. Different magnetic properties of the central metal (M = Ti, V) provide the difference in magnetic behavior of **1** and **2**. Salt **1** shows very large intermolecular antiferromagnetic interaction of $J/k_B = -123.0$ K. Complex **2** contains four spins in a $\{[V^{IV}OPc^{\bullet 3-}]^{\bullet-}\}_2$ π-stacking dimer. While the intermolecular antiferromagnetic interaction between the $Pc^{\bullet 3-}$ macrocycles in **2** is also strong as in **1**, the coupling between the V^{IV} and $Pc^{\bullet 3-}$ spins within one $[V^{IV}OPc^{\bullet 3-}]^{\bullet-}$ radical anion is essentially weaker. This data show that

intramolecular coupling between spins localized on paramagnetic metal centers and delocalized over the Pc$^{\bullet 3-}$ macrocycles is usually weak in $[(V^{IV}OPc^{\bullet 3-})]^{\bullet -}$. Similar tendency was found for $[Cu^{II}Pc^{\bullet 3-}]^{\bullet -}$.[20] At the same time, the intermolecular coupling between the Pc$^{\bullet 3-}$ macrocycles in the $\{[M^{IV}OPc^{\bullet 3-}]^{\bullet -}\}_2$ π-stacking dimers (M = Ti and V) can attain high values providing metal phthalocyanine compounds with effective magnetic coupling. As a future work, it is interesting to examine the generality of the tendency of strong and weak coupling between macrocycles and between metal and macrocycle, respectively.

ASSOCIATED CONTENT

Supporting Information: The IR spectra of starting compounds and **1** and **2**, magnetic data of **1** and **2**, and the results of DFT and TD-DFT calculations. This material is available free of charge via the Internet at http://pubs.acs.org.

AUTHOR INFORMATION

Corresponding Authors

*For D.V.K.: phone, +007-496-522-18-52; E-mail, konarev3@yandex.ru.

Notes

The authors declare no competing financial interest.

REFERENCES

(1) Claessens, C. G.; Blau, W. J.; Cook, M.; Hanack, M.; Nolte, R. J. M.; Torres, T.; Wöhrle, D. *Monat. Chem.* **2001**, *132*, 3–11.

(2) Wöhrle, D.; Schnurpfeil, G.; Makarov, S. G.; Kazarin, A.; Suvorova, O.N. *Macroheterocycles* **2012**, *5*, 191-202.

(3) Petersen, J. L.; Schramm, C. S.; Stojakovic, D. R.; Hoffman, B. M.; Marks, T. J. *J. Am. Chem. Soc*. **1977**, *99*, 286–288.

(4) Hasegawa, H.; Naito, T.; Inabe, T.; Akutagawa, T.; Nakamura, T. *J. Mater. Chem.* **1998**, *8*, 1567−1570.

(5) Matsuda, M.; Naito, T.; Inabe, T.; Hanasaki, N.; Tajima, H.; Otsuka, T.; Awaga, K.; Narymbetov, B.; Kobayashi, H. *J. Mater. Chem.* **2000**, *10*, 631-636.

(6) Matsuda, M.; Naito, T.; Inabe, T.; Hanasaki, N.; Tajima, H. *J. Mater. Chem.* **2001**, *11*, 2493-2497.

(7) Inabe, T.; Tajima, H. *Chem. Rev*. **2004**, *104*, 5503−5534.(8. Miller, J. S.; Vazquez, C.; Calabrese, J. C.; McLean, M. L.; Epstein, A. J. *Adv. Mater.* **1994**, *6*, 217-221.

(9) Rittenberg, D. K. ; Baars-Hibbe, L.; Böhm, A. B.; Miller, J. S. *J. Mater. Chem.* **2000**, *10*, 241-244.

(10) Tosatti, E.; Fabrizio, M.; Tóbik, J.; Santoro, G.E. *Phys. Rev. Lett.* **2004**, *93*, 117002.

(11) Lever, A. B. P.; Milaeva, E. R.; Speier, G.; In The phthalocyanines, properties and applications. Eds. Leznoff, C. C.; Lever, A. B. P.; **1993**, Vol. 3, VCH Publishing, Weinheim. Pages 1−69.

(12) Tahiri, M.; Doppelt, P.; Fischer, J.; Weiss, R. *Inorg. Chim. Acta* **1987**, *127*, L1−L3.

(13) Konarev, D. V.; Zorina, L. V.; Khasanov, S. S.; Hakimova, E. U.; Lyubovskaya, R. N. *New J. Chem.*, **2012**, *36*, 48-51

(14) Hückstädt, H.; Homborg, H. *Z. Anorg. Allg. Chem.* **1998**, *624*, 715−720.

(15) Konarev, D. V.; Zorina, L. V.; Ishikawa, M.; Khasanov, S. S.; Otsuka, A.; Yamochi, H.; Saito, G.; Lyubovskaya, R. N. *Cryst. Growth Des*. **2013**, *13*, 4930−4939.

(16) Konarev, D. V.; Khasanov, S. S.; Ishikawa, M.; Otsuka, A.; Yamochi, H.; Saito, G.; Lyubovskaya, R. N. *Inorg. Chem*. **2013**, *52*, 3851–3859

(17) Konarev, D. V.; Kuzmin, A. V.; Khasanov, S. S.; Lyubovskaya, R.N. *Dalton Trans*. **2013**, *42*, 9870–9876.

(18) Konarev, D. V.; Zorina, L. V.; Khasanov, S. S.; Litvinov, A. L.; Otsuka, A.; Yamochi, H.; Saito, G.; Lyubovskaya, R. N. *Dalton Trans.* **2013**, *42*, 6810–6816.

(19) Konarev, D. V.; Kuzmin, A. V.; Khasanov, S. S.; Otsuka, A.; Yamochi, H.; Saito, G.; Lyubovskaya, R. N. *Dalton Trans*. **2014**, *43*, 13061–13069.

(20) Konarev, D. V.; Kuzmin, A. V.; Faraonov, M. A.; Ishikawa, M.; Nakano, Y.; Khasanov, S. S.; Otsuka, A.; Yamochi, H.; Saito, G.; Lyubovskaya, R. N. *Chem. Eur. J.* **2015**, *21*, 1014–1028.

(21) Konarev, D. V. ; Troyanov, S. I. ; Ishikawa, M. ; Faraonov, M. A.; Otsuka, A. ; Yamochi, H.; Saito, G. ; Lyubovskaya, R. N. *J. Porph. Phth*. **2014**, *18*, 1157–1163.

(22) Wong, E. W. Y.; Leznoff, D. B. *J. Porph. Phth.* **2012**, *16*, 154–162.

(23) Wong, E. W. Y.; Walsby, C. J.; Storr, T.; Leznoff, D. B. *Inorg. Chem.* **2010**, *49*, 3343–3350.

(24) Cissell, J. A.; Vaid, T. P.; Rheingold, A. L. *Inorg. Chem.* **2006**, *45*, 2367–2369.

(25) Konarev, D. V.; Kuzmin, A. V.; Khasanov, S. S.; Otsuka, A.; Yamochi, H.; Saito, G.; Lyubovskaya, R. N. *Eur. J. Inorg. Chem.* 2016, 4099–4103.

(26) Cissell, J. A.; Vaid, T. P.; DiPasquale, A. G.; Rheingold, A. L. *Inorg. Chem.* 2007, *46*, 7713–7715.

(27) Zhou, W.; Platel, R. H.; Tasso, T. T.; Furuyama, T.; Kobayashi, N.; Leznoff, D. B. *Dalton Trans.* 2015, *44*, 13955–13961.

(28) Konarev, D. V.; Kuzmin, A. V.; Khasanov, S. S.; Ishikawa, M.; Otsuka, A.; Yamochi, H.; Saito, G.; Lyubovskaya, R. N. *Dalton Trans*. 2016, *45*, 10780−10788.

(29) Konarev, D. V.; Kuzmin, A. V.; Nakano, Y.; Faraonov, M. A.; Khasanov, S. S.; Otsuka, A. Yamochi, H.; Saito, G.; Lyubovskaya, R. N. *Inorg. Chem.* **2016**, *55*, 1390−1402.

(30) Konarev, D. V.; Khasanov, S. S.; Yudanova, E. I.; Lyubovskaya, R. N. *Eur. J. Inorg. Chem.* **2011**, 816−820.

(31) Tomachynsk, L. A.; Chernii, V. Ya.; Volkov, S. V. *Russ. J. Inorg. Chem.* **2002**, *47*, 208−211.

(32) Sheldrick, G. M. *Acta Crystallogr., Sect. A: Fundam. Crystallogr.* **2008**, *64*, 112−122.

(33) Yanai, T.; Tew, D.; Handy, N. *Chem. Phys. Lett.* **2004**, *393*, 51−57.

(34) Dunning, Jr., T. H. *J. Chem. Phys.* **1989**, *90*, 1007−1023.

(35) Balabanov, N. B.; Peterson, K. A. *J. Chem. Phys.* **2005**, *123*, 064107.

(36) NBO, Version 3.1, Glendening, E. D.; Reed, A. E.; Carpenter, J. E.; Weinhold, F.

(37) Gaussian 09, Revision D.01, Frisch, M. J.; Trucks, G. W.; Schlegel, H. B.; Scuseria, G. E.; Robb, M. A.; Cheeseman, J. R.; Scalmani, G.; Barone, V.; Mennucci, B.; Petersson, G. A.; Nakatsuji, H.; Caricato, M.; Li, X.; Hratchian, H. P.; Izmaylov, A. F.; Bloino, J.; Zheng, G.; Sonnenberg, J. L.; Hada, M.; Ehara, M.; Toyota, K.; Fukuda, R.; Hasegawa, J.; Ishida, M.; Nakajima, T.; Honda, Y.; Kitao, O.; Nakai, H.; Vreven, T.; Montgomery, Jr., J. A.; Peralta, J. E.; Ogliaro, F.; Bearpark, M.; Heyd, J. J.; Brothers, E.; Kudin, K. N.; Staroverov, V. N.; Keith, T.; Kobayashi, R.; Normand, J.; Raghavachari, K.; Rendell, A.; Burant, J. C.; Iyengar, S. S.; Tomasi, J.; Cossi, M.; Rega, N.; Millam, J. M.; Klene, M.; Knox, J. E.; Cross, J. B.; Bakken, V.; Adamo, C.; Jaramillo, J.; Gomperts, R.; Stratmann, R. E.; Yazyev, O.; Austin, A. J.; Cammi, R.; Pomelli, C.; Ochterski, J. W.; Martin, R. L.; Morokuma, K.; Zakrzewski, V. G.; Voth, G. A.; Salvador, P.; Dannenberg, J.; Dapprich, J. S.; Daniels,

A. D.; Farkas, O.; Foresman, J. B.; Ortiz, J. V.; Cioslowski, J.; Fox, D. J., Gaussian, Inc., Wallingford CT, 2009.

(38) Konarev, D. V.; Khasanov, S. S.; Otsuka, A.; Maesato, M.; Saito, G.; Lyubovskaya, R. N. *Angew. Chem. Int. Ed.* **2010**, *49*, 4829–4432/

(39) Konarev, D. V.; Khasanov, S. S.; Otsuka, A.; Maesato, M.; Uruichi, M.; Yakushi, K.; Shevchun, A.; Yamochi, H.; Saito, G.; Lyubovskaya, R. N. *Chem. Eur. J.* **2014**, *20*, 7268–7277.

(40) Whangbo, M. -H.; Hoffmann, R. *J. Am. Chem. Soc.* **1978**, *100*, 6093–6098.

(41) Crystal and Electronic Structure Analysis Using CAESAR,   Ren, J.; Liang, W.; Whangbo, M. -H. **1998**, Prime Color Software, Inc. (this book can be downloaded free of charge from the website: http://www.PrimeC.com/). Default parameters were used.

(42) Oka, K.; Okada, O.; Nukada, K. *Jpn. J. Appl. Phys.* **1992**, *31*, 2181–2184/

(43) Okada, O.; Oka, K.; Iijima, M. *Jpn. J. Appl. Phys.* **1993**, *32*, 3556–3560.

(44) Yamaguchi, K.; Takahara, Y.; Fueno, T.; Nasu, K. *Jpn. J. Appl. Phys*. **1987**, *26*, L1362–L1364.

(45) Smart, J. S. In Magnetism III, Eds by Rado, G. T.; Suhl, H. Academic Press, NY, **1963**, p. 63.

 (46) Liu, Z. -L.; Li, Liao, D. -Z.; Jiang, Z. -H.; Yan, S. -P. *Cryst. Growth Des*. **2005**, *5*, 783–787.

(47) (a) Assour, J. M.; Goldmacher, J.; Harrison, S. E. *J. Chem. Phys.* **1965**, *43*, 159–165.

(48) Özçesmeci, I.; Yerli, Y.; Okur, A. - I.; Gül, A. *Inorg. Chem. Commun*. **2009**, *12*, 625–627.

(49) Kivelson, D.; Lee, S.-K. *J. Chem. Phys.* **1964**, *41*, 1896–1903.

(50) Sato, M.; Kwan *T. J. Phys. Chem.* **1969**, *50*, 558–559.

(51) Handa, M.; Suzuki, A.; Shoji, S.; Kasuga, K.; Sogabe, K. *Inorg. Chim. Acta* **1995**, *230*, 41–44.

For Table of Contents Use Only

Magnetic and optical properties of layered $(Me_4P^+)[M^{IV}O(Pc^{•3−})]^{•−}(TPC)_{0.5}·C_6H_4Cl_2$ salts (M = Ti and V) composed of π-stacking dimers of titanyl and vanadyl phthalocyanine radical anions

D.V. Konarev, Y. Nakano, S. S. Khasanov, A. V. Kuzmin, M. Ishikawa, A. Otsuka, H. Yamochi, G. Saito, R. N. Lyubovskaya

GRAPHIC:
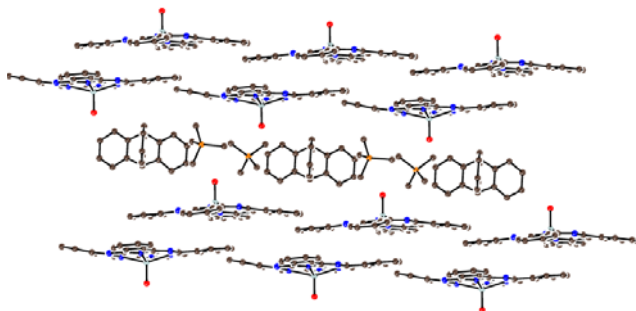
SYNOPSIS :

Salts with radical anions of titanyl and vanadyl phthalocyanines $(Me_4P^+)[M^{IV}O(Pc^{•3−})]^{•−}(TPC)_{0.5}·C_6H_4Cl_2$ (M = Ti (**1**), V (**2**)) have been obtained. They contain the $[(M^{IV}OPc^{•3−})^{•−}]_2$ dimers in which strong coupling between $Pc^{•3−}$ is realized. Salt **2** contains additional spin on V^{IV} while the intramolecular magnetic coupling between V^{IV} and $Pc^{•3−}$ is essentially weak.